The Ultra-high Hg^0 Adsorption Capacity Modified by Selenium

Ye Liu
East China University of Science and Technology
Chenglong Ma
East China University of Science and Technology
Jiacheng Zhou
East China University of Science and Technology
Lin Zhu
East China University of Science and Technology
Limei Cao
East China University of Science and Technology
Ji Yang (yangji@ecust.edu.cn)
East China University of Science and Technology https://orcid.org/0000-0002-5209-7436

Research Article

Keywords: mercury removal, elemental mercury, carbon-based sorbent, selenium

Posted Date: February 24th, 2022

DOI: https://doi.org/10.21203/rs.3.rs-1298241/v1

Abstract

Activated carbon was one of the main adsorptions utilized in elemental mercury (Hg^0) removal from coal combustion flue gas. However, the high cost and low physical adsorption efficiency of activated carbon injection (ACI) limited its application. In this study, an ultra-high efficiency catalyst sorbent-Se_x/Activated carbon (Se_x/AC) was synthesized and applied to remove Hg0 in the simulated flue gas, which exhibited 120 times outstanding adsorption performance versus the conventional activated carbon. The Se_x/AC reached 17.98 mg/g Hg^0 adsorption capacity at 160 °C in a pure nitrogen atmosphere. Moreover, it maintained an excellent mercury adsorption tolerance at the NO and SO_2 conditions in a bench-scale fixed-bed reactor. Characterized by the multiple methods, including BET, XRD, XPS, and the DFT calculation, we demonstrated that the ultrahigh mercury removal performance was driven from the activated Se species in Se_x/AC. Chemical adsorption was the main reason for Hg^0 removal: Selenium on the surface of AC would capture Hg^0 in the flue gas to form an extremely stable substance-HgSe, avoiding subsequent Hg^0 released. Additionally, the oxygen-containing functional groups in AC and the higher BET areas promote the conversion of Hg^0 to HgO. This work provided a novel and highly efficient carbon-based sorbent -Se_x/AC to capture the mercury in coal combustion flue gas.

1. Introduction

Coal combustion has caused severe environmental pollution. Mercury is a kind of toxic heavy metal, which widely exists in coal combustion flue gas in the form of mercury vapor, and it has resulted in the extreme negative on environment and humungous damage to human's health owing to the chemical activity (highly toxic, high stability, bioaccumulation, persistence, and long-distance migration) and toxic Hg-based derivative(Reddy et al., 2012). According to UNEP's global mercury assessment report in 2018, human activities have increased total atmospheric mercury concentrations up to 450% natural level. Coal combustion flue gas is the main anthropogenic emission source, accounting for 21%, and this number is still increasing(Outridge et al., 2018). In general, there are three types of mercury in flue gas: particle-bound mercury (Hg^p), oxidized mercury (Hg^{2+}), and elemental mercury(Hg^0)(Yang et al., 2018). Hg^p and Hg^{2+} can be removed by a dust collector and wet desulfurization device in the flue gas treatment facilities, respectively. However, Hg^0 is hard to be removed by the general device owing to its high volatility, chemical inertness, and insolubility(Liu & Wang, 2014; Zhou et al., 2019). Thus, there is an urgent need for efficient and cost-effective removal techniques for Hg^0.

Currently, catalytic oxidation(Li et al., 2010; Xu et al., 2017), photochemical oxidation(Liu et al., 2014; Zhao et al., 2018), and adsorption(Z. Liu et al., 2019) are common methods to remove Hg^0. Adsorption technology has been widely used due to its simple operation, strong stability, and less secondary pollution(Liu et al., 2020; Yang et al., 2007). In conventional adsorptions, activated carbon injection (ACI) is one of the most effective and widely used technology for Hg^0 removal owing to its large specific surface and sufficient surface oxygen functional groups(Fan et al., 2016; Krishnan et al., 1994).

Nonetheless, raw activated carbon (R-AC) also has some disadvantages, such as high operation cost and limited effect(Sun et al., 2017). At present, increasing the surface active sites is the most effective method of activated carbon (AC) modification, including halide modification(Qu et al., 2016; Tong et al., 2017; Zhong et al., 2017), acid and alkali modification(Zheng et al., 2017), sulfur modification(Sano et al., 2017; Yao et al., 2014), metal and metal oxides modification(S. Yang et al., 2019; Zhu et al., 2018), and plasma modification(Zhang et al., 2016). However, the above methods still have the problem of low Hg^0 removal efficiency. Consequently, it is necessary to develop a more efficient and valuable modification method of AC.

Selenium (Se) shows excellent chemical combination ability in removing mercury. The binding affinity constant of mercury and selenide is 10^{22}, which is one million-fold higher than that the binding affinity between mercury and sulfur(Ahmed et al., 2017). Selenium can combine with gaseous mercury to form an extraordinarily stable mercury selenide (HgSe) precipitate, with solubility constant (K_{sp}, 1.0×10^{-59}) as compared to that of HgSn (K_{sp}, 1.0×10^{-52}), avoiding the risk of leaching hazardous in subsequent processing(Ahmed et al., 2017; J. Yang et al., 2019). Previous research(J. Yang et al., 2020; J. Yang et al., 2019; Z. Yang et al., 2020) has established that selenium or selenide as an active component plays a key role in the removal of Hg^0. Yang et al. selected MIL-101(J. Yang et al., 2019) and copper foam(J. Yang et al., 2020) as the supporters for selenium particles. These two adsorbents show excellent Hg^0 adsorption capacity. However, the synthesis process using MIL-101 or copper foam as a carrier is complex and has not been widely used in commercial applications compared with AC. Furthermore, AC is a better material owning to its larger specific surface area, better pore structure and porosity, more active site on the surface, and higher consistency with the current industrial application. Therefore, it is a cost-effective and prospective option to select AC as a carrier of selenium.

In this study, the different proportions of selenium activated carbon adsorbent were synthesized by a simple high temperature selenium impregnation method. The Hg^0 removal efficiency was systematically evaluated under different conditions (reaction temperature and gas composition). The new adsorbent has more than ten times the adsorption capacity than R-AC. Meanwhile, according to the DFT calculation and samples characterization analysis, the mechanism of removing Hg^0 by the samples is explored. The synergistic effect of physical adsorption caused by AC and chemical adsorption caused by Se provides high Hg adsorption efficiency.

2. Materials And Methods

2.1 Synthesis of sorbent

In this study, the sample of Se_x/AC is synthesized by high-temperature selenium impregnation through the following three steps. The first step is to pretreat AC. The AC particles (20-50 mesh) are chosen as the carrier. Firstly, the AC is sonicated with ethanol for 30 min to remove the impurities, and then rinse the AC with deionized water several times. Afterward, the AC is dried at 120°C overnight in an oven and

designated as R-AC. The second step is to synthesize the sample (Se_x/AC). In this procedure, 0.4g R-AC is thoroughly mixed with 0.4g selenium powder to obtain a completely homogeneous mixture. Then, the mixture is calcined in the tube furnace at 300℃ for 3 h. Before starting the calcination, inert gas is blown in for 20 min and kept during the process. The last step of this procedure is the activated treatment of the sample. After removal from the tube furnace, the mixture is put into the muffle furnace for 3 h, where it preheats to 300℃. After cooling to room temperature, the final sample is obtained (denoted as Se_1/AC). Reducing selenium powder to 0.2 g and 0.1 g, $Se_{0.5}$/AC, and $Se_{0.25}$/AC are synthesized by the same method while other parameters were fixed.

2.2 Characterization of sample

The Brunauer-Emmett-Teller (BET) method is used to measure the specific area and porosity of all samples by the instrument (Micromeritics Tristar 3020 SIN 993) at -196°C by N_2 adsorption and desorption. The crystal structure of the samples is characterized by X-ray diffraction (XRD, D/Max 2550VB, Cu Kα, λ = 1.5046Å, 18kV)at 10-80°. The surface microcosmic morphology of all samples is analyzed by scanning electron microscope (SEM, S-3400N) and energy-dispersive spectroscopy (EDS). The chemical states of surface elemental are measured by X-ray photoelectron spectroscopy (XPS, ESCALAB 250Xi, Al kα, hυ = 1486.6eV). The mercury species on the used Se_x/AC surface is identified by Temperature-Programmed-Decomposition (TPD). During the TPD process, the sample raises from 25°C to 650°C at a rate of 5°C·min^{-1} in the 0.5L·min^{-1} pure nitrogen.

2.3 Experimental setup and procedure

The mercury removal performance of the prepared Se_x/AC samples is tested in a fixed bed reactor. The experimental setup consisted of the gas supply system (O_2, N_2, SO_2, NO), mercury vapor generator, constant temperature water bath, digital mercury detector (SG-921, Jiangsu Jiangfen Electroanalytical Instrument Co., Ltd., China), electric heating furnace, and data acquisition computer. The quartz tube (length 4000mm, inner diameter 10mm) is where the sorbent is placed, and the mercury vapor will be removed. The quartz tube is filled with roughly 50mg Se_x/AC sample, both ends are secured with 10mm quartz wool, and the quartz tube is then placed in the electric heating furnace and linked to the fixed bed reaction equipment. Potassium permanganate solution is set at the end of the experimental device as the tail gas treatment device to discharge the exhaust gas into the atmosphere after treatment.

In the experiment, the gas flow rate is set to 100mL/min, the calculated space velocity of 6100 h^{-1}, and the sample mass used in the process is 50mg. Before the start of each experiment, pass the mixed gas of N_2 and mercury vapor through the mercury measuring instrument, adjust the temperature of the water bath to reach the required concentration, and wait until the mercury vapor concentration stabilizes (within 30 min, the fluctuation do not exceed 5%). As a tail gas treatment device, a potassium permanganate solution gas washing bottle is installed at the end of the experimental system. The digital mercury detector is used to determine the concentration of mercury vapor at the exit. The formulas for calculating mercury removal rate “η, %” Eqs. (1) and adsorption capacity “a” Eqs. (2) are as follows:

$$\eta = \frac{C_{in}-C_{out}}{C_{in}} \times 100\% \quad \text{Eqs. (1)}$$

$$a = \frac{(C_{in} \times t - \int_0^t C_{out} dt) \times q}{m} \quad \text{Eqs. (2)}$$

where C_{in} and C_{out} (μg/m^3) are the mercury input and output concentrations, respectively; t (min) is the adsorption time; q (m^3/min) is the gas total flow rate; m (g) represents the weight of the sample.

The sample invalided is recorded when 10% penetration is attained and the experiment is terminated. (10 percent penetration: and C_{out} reached 10 percent of the C_{in}). The time when the penetration rate reaches 10% is recorded as the penetration time.

3. Result And Discussions

3.1 Characterization

The specific surface area and the pore structure parameters of all samples is calculated by BET. The N_2 adsorption and desorption isotherm tests are carried out on R-AC and Se_x/AC samples to evaluate the porosity. The adsorption-desorption curves are shown in Fig. 1a. All samples had reversible type isotherms, which is one of the chief characteristics of mesoporous materials. It can be seen that the pore structure parameters decreased with increasing selenium from Fig. 1b. As shown in Fig. 1b and 1c, the BET surface area and pore volume of R-AC are 783.52 m^2/g and 0.17cm^3/g, which are higher than that of $Se_{0.25}$/AC (530.42 m^2/g, 0.15cm^3/g), $Se_{0.5}$/AC (481.73m^2/g, 0.12cm^3/g) and Se_1/AC (453.64m^2/g, 0.11cm^3/g) after modification by selenium, and from Fig. 1c, the selenium contents of $Se_{0.25}$/AC, $Se_{0.5}$/AC and Se_1/AC was 3.62 wt%, 15.29 wt% and 24.64 wt%, respectively. It indicated that with the increase of selenium loading, the BET surface area decreases. The reason is that the selenium blocked part of the pores of AC during the loading process. As the BET surface area and pore volume of sorbent decrease, the effect of physical adsorption in the experiment is weakened. When combined with the subsequent Hg^0 removal experiment result (Fig. 4b), it can be concluded that the adsorption capacity is enhanced when the BET surface area of the AC decreases by selenium loading. Therefore, we speculate that selenium provided more chemically active adsorption sites than AC in the process of Hg^0 removal.

The XRD patterns of all prepared samples are shown in Fig. 1d. The measured samples only show two broad diffraction peaks at 26° and 43°, which correspond to the amorphous carbon peak(Danmaliki & Saleh, 2017). These two peaks are semi-crystalline pores caused by carbon decomposition along the direction of graphitic structures(S. Yang et al., 2019). The obvious diffraction peak of Se is not detected in the XRD spectrum of AC samples after selenium impregnation, which indicates that Se exists in the amorphous form in Se_x/AC or is highly dispersed on the surface of AC.

The SEM images of R-AC and $Se_{0.5}$/AC were shown in Fig. 2, and the microscopic morphology of the sorbent can be clearly observed. Fig. 2a showed that there are many channels on the surface of AC particles, and they can enhance the Hg^0 adsorption capacity of AC. Fig. 2b shows that the selenium is successfully loaded onto AC, and has a uniform dispersion on the surface of AC, which is consistent with the XRD findings. Comparing Fig. S1a and b, the process of high temperature selenium impregnation does not change the granularity of the AC. However, the loading of selenium blocked part of AC pore channels, which explains the decrease of specific surface area with the loading of selenium in the BET test. As shown in Fig. S2c and d, after the Hg^0 adsorption experiment, the morphology of $Se_{0.5}$/AC changes significantly, and the structure of AC is destroyed. The particle size becomes small, and the combination of Se and Hg^0 further blocks the pores of AC. It indicates that the maintenance of the adsorbent's overall structure ensures efficient removal of Hg0, and when the structure is disrupted, the selenium still exists, but the effect of Hg^0 removal is diminished.

3.2 Hg^0 removal performance

The 12-hour Hg^0 removal experiment is performed at 25°C under nitrogen. The experimental device and the progess were presented in Fig. 3. The result in Fig. 4a indicates that the efficiency of the mercury removal from the sample is significantly increased after the loading of selenium compared to that of R-AC. When R-AC is used as an adsorbent, the penetration point is reached within 80 min, while the Se_x/AC shows a very excellent mercury adsorption capacity that can reach nearly 100% adsorption efficiency within 30 min and remain above 85% within 12h. The adsorption efficiencies of Se_1/AC and $Se_{0.5}$/AC are maintained at 93%.

The mercury adsorption penetration experiments are conducted at 25°C under N_2 conditions to accurately evaluate the mercury adsorption capacity of Se_x/AC samples, and the results are shown in Fig. 4b. It can be seen that the longest effective time is recorded by $Se_{0.5}$/AC with 34.60h, while $Se_{0.25}$/AC and Se_1/AC have penetration times of 12.75h and 29.25h, respectively. According to Eqs. (2), the mercury adsorption capacities of R-AC, $Se_{0.25}$/AC, $Se_{0.5}$/AC and Se_1/AC are calculated to be 0.15mg/g, 1.42mg/g, 4.04mg/g and 3.40mg/g, respectively. The adsorption capacity also indicates that the selenium-modified AC is substantially improved, reaching 9.47~26.93 times of the R-AC. Comparing the three Se_x/AC samples, the $Se_{0.5}$/AC is selected for the subsequent experiments with the largest adsorption capacity.

3.2.1 Effect of temperature on Hg^0 removal

In order to investigate the effect of temperature on the mercury removal effect of Se_x/AC, the temperature of 80°C, 120°C, 160°C, 200°C is chosen in the mercury removal experiment and the result is shown in Fig. 4c. Initially, the removal efficiency of mercury is above 90% at each temperature condition. Continuing to increase the experiment time to reach 10% penetration point (Fig. 4d), the adsorption efficiency shows a trend of increasing and then decreasing with the increase of temperature. The adsorption capacity is 4.04mg/g, 4.92mg/g, 9.42mg/g, 17.98mg/g and 15.67mg/g, respectively. Thus,

the optimal temperature range is around 160°C. During the adsorption process, the increase of temperature stimulates the chemisorption of the sorbent, while the physical adsorption is inhibited(Qiu et al., 2017). Based on the results of the experiment at different temperatures, it can be concluded that chemisorption occupied an important position in this study, which is the same as the result of BET. When the temperature is higher than 160°C, the adsorption capacity decreases because the chemical bond is broken in high temperatures during the chemisorption process, which affects the formation of Hg-Se. Meanwhile, the selenium-mercury combination melts, and the liquid selenium-mercury combination blocks the pore channels of the sorbent, which affects the adsorption process(Jurng et al., 2002; Yan et al., 2004).

3.2.2 Effect of O_2 on Hg^0 removal

In the actual flue gas treatment, Hg^0 removal is carried out under air conditions, so it is a question worth investigation that whether the presence of oxygen affects the efficiency of removal of Hg^0 of Se_x/AC. The experiment is conducted under the inlet gas conditions containing 3%, 6%, 9%, and 21% O_2 (the rest of the composition is N_2), and the results are shown in Fig. 4e. The Hg^0 removal efficiency is close between different oxygen ratios, and the time to reach the penetration point is 54.77h, 58.68h, 56.68h, and 56.92h, respectively. But they are all lower than that of nitrogen. Selenium had strong antioxidant properties(Cai et al., 2012), and selenium loaded on AC will react with Hg^0 to form HgSe. Fig. 5d (used Se 3d) shows that SeO_2 is still produced under pure nitrogen. It indicates that when oxygen is involved, competition between oxygen and Hg^0 occurs and the part of selenium reacting with Hg^0 decreases. Thus, it reduces the efficiency of the removal of Hg^0 by Se_x/AC.

3.2.3 Effect of NO and SO_2 on Hg^0 removal

Typically, the presence of NO and SO_2 in coal combustion flue gas has an impact on the removal of Hg^0. Therefore, this paper explores the mercury adsorption efficiency of Se_x/AC in the presence of NO and SO_2. As shown in Fig. 4f, the adsorption efficiency of Se_x/AC decreases in N_2+NO or N_2+ SO_2 compared to pure N_2 conditions. Within 24h experiment, the Hg^0 removal efficiency decreases from 97.37–92.51% under NO atmosphere and from 98.61–86.12% under SO_2. This suggests that SO_2 had a toxic effect on the adsorption of Hg^0 because the SO_2 molecule combined with the oxygen-containing functional groups on the adsorption surface, competing with Hg^0 and inhibiting the adsorption effect of Hg^0 (Presto & Granite, 2007). Although NO and SO_2 inhibit the adsorption of Hg^0 by Se_x/AC, the efficiency is maintained at over 85%. Thus Se_x/AC is an efficient Hg^0 adsorption that can protect against NO and SO_2.

3.3 Hg^0 removal mechanism of Se_x/AC

The detailed chemical characteristics of elements in fresh and used $Se_{0.5}$/AC samples are analyzed by XPS. Fig. 5a shows the full spectrum of the fresh $Se_{0.5}$/AC. It can be seen that selenium is successfully loaded on the surface of AC, which is consistent with the EDS test result. The peak of C1s at 284.77eV,

285.59 eV, 286.63 eV, and 288.54 eV are attributed to C-C, C-O, C=O, and COOH, respectively(Puziy et al., 2008). Table 2 shows the changes in the relative intensity of each functional group in C1s. Compared with fresh samples, the relative content of C-C increases from 60.08–70.85%, and the relative strength of oxygen functional groups (C-C, C-O, C=O, and COOH) decreases from 39.92–29.15%. It indicates that the oxygen functional groups in $Se_{0.5}$/AC can promote the adsorption of Hg^0 (Li et al., 2002). Hg^0 will combine with these functional through the complex electron transfer process and attach to the surface of $Se_{0.5}$/AC in the form of Hg^{2+}. As shown in Fig. 4e, Se 3d fitting curve of the fresh sample illustrates two strong peaks at 55.9 eV and 56.86 eV for $Se3d_{5/2}$ and $Se3d_{3/2}$, respectively(S. Liu et al., 2019). In Fig. 5d, the blind energy of Se3d of the used sample moves to a lower region. It reveals that Se on the sample surface changes from elemental selenium to Se^{2-} during the process of removal Hg^0. Meanwhile, a new peak (59.1eV) appears in the Se 3d curve in Fig. 4f that is attributed to $SeO_{2(S. Liu et al., 2019)}$, indicating that selenium reacts with oxygen. Because the experiment is carried out under pure nitrogen, it is proved that the oxygen-containing functional groups in AC not only participate in the oxidation process of Hg^0, but also oxidize part of Se. It can be seen from Fig. 5d that the Hg 4f spectra for both used R-AC and $Se_{0.5}$/AC show two peaks. The peak at 101.6 eV and 101.1 eV corresponded to $Hg4f_{7/2}$, and 105.53 eV and 107.76 eV are attributed to $Hg4f_{5/2}$. The XPS results of Hg4f confirm the existence of Hg^{2+} on the surface of the used samples(Tao et al., 2012). On the surface of R-AC, Hg^{2+} mainly exists in the form of HgO, which is consistent with the XPS result of C1s, while on the surface of $Se_{0.5}$/AC it is mainly HgSe, which agree with the XPS result for Se3d.

Table 2
the relative intensity of functional groups in C1s

Functional group	Relative intensity (%)	
	Fresh	Used
C-C	60.08	70.85
C-O	15.06	10.74
C=O	9.48	8.38
COOH	15.38	10.03
Oxygen functional group	39.92	29.15

In order to explore the Hg^0 removal mechanism of Se_x/AC, Hg-TPD is carried out to determine the mercury species. As the result of Hg-TPD shown in Fig. 5b, it can be seen that two peaks appear at 320°C and 530°C respectively with the increase of temperature. The desorption peak around 320°C is contributed to HgSe(J. Yang et al., 2019). In addition, the peak around 530°C can correspond to HgO which is generated by the interaction of Hg^0 and oxygen-containing functional groups in AC. The peak of physisorption is not occurred (around 110°C)(Sun et al., 2017). The result of TPD further confirms that the mercury species on the Se_x/AC surface are mainly HgSe and HgO, which is consistent with the previous XPS analysis.

3.4 Calculation method and the model

In order to further explore the adsorption capacity, the density functional theory (DFT) calculation was conducted by using the Vienna Ab-initio Simulation Package (VASP) in this work. The generalized gradient approximation with PBE functional and the projector-augmented wave (PAW) method was adopted. The energetic convergence threshold for the self-consistent field (SCF) was set to 1×10^{-5} eV/atom, and the force threshold was set to 0.02 eV/Å. According to the investigation in Fan's work(Fan et al., 2016), we could draw the conclusion that the adsorption behavior of Hg on pure activated carbon is physical adsorption. In addition, we assume that there is no significant electronic interaction between Se and activated carbon because of the non-nano scale particle size of selenium. Therefore, we considered the adsorption behavior of Hg atom on the Se slab model. The XRD pattern of the Se powder utilized in this work was provided in Fig. 6a. According to the XRD results of Se powder, the highly exposed (101) face plane (2×2 supercell) was considered in the construction of a 4-layer slab model with a 15 Å vacuum region. The bottom two layers were fixed, and the top two layers were allowed to relax. Since the HgSe have the F-43m space group, therefore a bridge adsorption model was constructed and structurally optimized. The adsorption model is provided in Fig. 6b. The optimized bond of Hg-Se equals 2.51 Å, which is lower than the Hg-Se bond distance of 2.72Å in the HgSe crystal. Such a conclusion represents that adsorption is dominated by chemical adsorption.

Considering the interaction among the valence electron orbital of Hg s state and Se p state. The partial density of states (PDOS) for the Hg s state and Se p state were presented in Figure 6c. The localized Hg s state of the gaseous Hg atom turns to be delocalized Hg s state on the Se-slab distributing on both sides of the Fermi level ($E-E_f = 0$), which represents the σ bond formation between the Hg-Se. In the PDOS of the Se p state, the delocalized p_z represents the interaction with the Hg s state. In the Bader charge of the Hg s state, the calculated -0.3 electrons have confirmed the electron transfer from the Hg s state to Se p state.

The adsorption energy calculation formula is provided in the following equation

$$E_{ads}\,(Hg) = E_{(Se-slab-101-Hg)} - E_{(Hg)} - E_{(Se-slab-101)} \quad (1)$$

where $E_{(Se-slab-101-Hg)}$ is the total energy of the Se-slab-(101) with a single Hg atom in its equilibrium condition, which equals -162.0139 eV. $E_{(Hg)}$ is the total energy of the single gaseous Hg atom, which equals -0.0294 eV. $E_{(Se-slab-101)}$ is the total energy of the Se-slab-(101) model, which equals -162.8895 eV. Therefore, the E_{ads} (Hg) equals -0.8462 eV (-81.5059 kJ/mol).

Such a value is extremely lower than the adsorption energy of transition metal-loaded activated carbon(Fan et al., 2016) (Table S2), which demonstrates the strong chemical adsorption capacity of Se.

3.5 Adsorption mechanism

According to the above experiment results and characterization analysis, the mechanism of Hg^0 removal over Se_x/AC can be explained by two steps. The first step is physical adsorption. Due to the physical properties of AC, such as excellent pore structure, the Hg^0 is adsorbed onto the surface of AC as it passes through (Eqs. 3). With the temperature rising, the effect of physical adsorption is gradually inhibited, while the chemisorption is significantly enhanced for the adsorption of Hg^0. The second step is chemical adsorption. A part of Hg(ad) will be captured by the oxygen-containing functional groups (C-O, C=O, COOH) in AC and forms HgO (Eqs. 4). Meanwhile, a portion of selenium loaded on AC will form a chemical bond with the Hg^0 atom. Most of the selenium will convert Hg(ad) into HgSe by chemical adsorption, accompanied by electron transfer (Eqs. 5). Thus, it can be seen that AC will only provide a larger specific surface area for selenium and increase the probability of binding selenium and Hg^0, while chemical adsorption dominates the Hg^0 removal process. The main reactions are as follows:

$$Hg^0(g) + AC \rightarrow Hg(ad) \quad \text{Eqs. 3}$$

$$Hg(ad) + AC\text{-}O \rightarrow HgO + C \quad \text{Eqs. 4}$$

$$Hg(ad) + Se \rightarrow HgSe + C \quad \text{Eqs. 5}$$

4. Conclusions

In this study, selenium-loaded activated carbon (Se_x/AC) is prepared by high temperature selenium impregnation method for the removal of Hg^0 from coal-fired flue gas. The composite component achieves strong physical adsorption and chemical adsorption. AC provided a larger specific surface area for selenium, exposing more active sites for Hg^0 binding. Uniformly dispersed Se on the surface of AC could capture the Hg^0 in the flue gas and facilitate the formation of HgSe by chemical adsorption. Based on the results of Hg^0 adsorption experiment, $Se_{0.5}$/AC shows the best efficiency. Under optimal conditions ($Se_{0.5}$/AC, 160°C, pure N_2), it can maintain more than 90% mercury removal efficiency within 154.75h, and the adsorption capacity is 17.98mg/g. Moreover, the adsorbent has excellent anti toxicity to NO and SO_2 (the Hg^0 removal efficiency is more than 85% within 24h). SEM result revealed that Hg^0 removal efficiency is limited by the structure destruction of the adsorption. Through the analysis of XPS, Hg-TPD, and the DFT adsorption model calculation, the final mercury species formed are mainly HgSe and HgO. In a suitable temperature range, selenium can capture Hg^0 in flue gas through chemical adsorption to form HgSe, and the oxygen-containing functional groups in AC also paly an oxidizing role for Hg^0 removal to form HgO. Hence, Se_x/AC has broad prospects in the practical application of flue gas mercury removal.

Declarations

Acknowledgment

Thanks to the Research Center of Analysis and Test of East China University of Science and Technology for the help on materials characterization analysis.

Funding

This work is supported by the National Natural Science Foundation of China (51778229) and the Fundamental Research Funds for the Central Universities (JKB012015019).

Data availability

The data and materials used and analyzed during the study are available in this published article.

Compering interests: The authors declare no conflict of interest.

Consent of publication: Informed consent for publication was obtained from all participants.

Ethics approval and consent to participate: Not applicable

Corresponding Author

Ji Yang - School of Resources and Environmental Engineering, East China University of Science and Technology, 130 Mei Long Road, Shanghai 200237, China; ORCID: https://orcid.org/0000-0002-5209-7436; Email: yangji@ecust.edu.cn

Authors

Ye Liu - School of Resources and Environmental Engineering, East China University of Science and Technology, 130 Mei Long Road, Shanghai 200237, China; Email: Ecustly19@126.com

Cheng-Long Ma - School of Resources and Environmental Engineering, East China University of Science and Technology, 130 Mei Long Road, Shanghai 200237, China; ORCID: https://orcid.org/0000-0003-2879-1169; Email: kuailelong101@163.com

Jia-Cheng Zhou - School of Resources and Environmental Engineering, East China University of Science and Technology, 130 Mei Long Road, Shanghai 200237, China; Email: zhoujiacheng199416@163.com

Lin Zhu - School of Resources and Environmental Engineering, East China University of Science and Technology, 130 Mei Long Road, Shanghai 200237, China; Email: jsdzhulin@163.com

Li-Mei Cao - School of Resources and Environmental Engineering, East China University of Science and Technology, 130 Mei Long Road, Shanghai 200237, China; ORCID: https://orcid.org/0000-0001-7642-4756; Email: caolimei@ecust.edu.cn

Author contribution

L Y and Y J are the experimental designers; L Y performed the experimental; L Y, Z JC and C LM contributed significantly to analysis and manuscript preparation; L Y and M CL completed data analysis and worte the manuscript; Z L and C LM helped perform the analysis with contructive dis cussions.

References

1. Ahmed S, Brockgreitens J, Xu K, Abbas A (2017) A Nanoselenium Sponge for Instantaneous Mercury Removal to Undetectable Levels. Adv Funct Mater 27(17) Article 1606572. https://doi.org/10.1002/adfm.201606572
2. Cai SJ, Wu CX, Gong LM, Song T, Wu H, Zhang LY (2012) Effects of nano-selenium on performance, meat quality, immune function, oxidation resistance, and tissue selenium content in broilers. Poult Sci 91(10):2532–2539. https://doi.org/10.3382/ps.2012-02160
3. Danmaliki GI, Saleh TA (2017) Effects of bimetallic Ce/Fe nanoparticles on the desulfurization of thiophenes using activated carbon. Chem Eng J 307:914–927. https://doi.org/10.1016/j.cej.2016.08.143
4. Fan L, Ling L, Wang B, Zhang R (2016) The adsorption of mercury species and catalytic oxidation of Hg0 on the metal-loaded activated carbon. Appl Catal A 520:13–23. https://doi.org/10.1016/j.apcata.2016.03.036
5. Jurng J, Lee TG, Lee GY, Lee SJ, Kim BH, Seier J (2002) Mercury removal from incineration flue gas by organic and inorganic adsorbents. Chemosphere 47(9):907–913 Article Pii s0045-6535(01)00329-0. https://doi.org/10.1016/s0045-6535(01)00329-0
6. Krishnan SV, Gullett BK, Jozewicz W (1994) Sorption of elemental mercury by activated carbons. Environ Sci Technol 28(8):1506–1512. https://doi.org/10.1021/es00057a020
7. Li J, Yan N, Zan Q, Qiao S, Jia J (2010) Catalytic oxidation of elemental mercury over the modified catalyst Mn/alpha-Al2O3 at lower temperatures. Environ Sci Technol 44(1):426–431
8. Li YH, Lee CW, Gullett BK (2002) The effect of activated carbon surface moisture on low temperature mercury adsorption. Carbon 40(1):65–72. https://doi.org/10.1016/s0008-6223(01)00085-9
9. Liu D, Li C, Wu J, Liu Y (2020) Novel carbon-based sorbents for elemental mercury removal from gas streams: A review. Chem Eng J 391. https://doi.org/10.1016/j.cej.2019.123514
10. Liu S, Wang M, Qian T, Liu J, Yan C (2019) Selenium-Doped Carbon Nanosheets with Strong Electron Cloud Delocalization for Nondeposition of Metal Oxides on Air Cathode of Zinc-Air Battery. ACS Appl Mater Interfaces 11(22):20056–20063. https://doi.org/10.1021/acsami.9b04870
11. Liu Y, Pan J, Wang Q (2014) Removal of Hg0from containing-SO2/NO flue gas by ultraviolet/H2O2process in a novel photochemical reactor. AIChE J 60(6):2275–2285. https://doi.org/10.1002/aic.14388
12. Liu Y, Wang Q (2014) Removal of elemental mercury from flue gas by thermally activated ammonium persulfate in a bubble column reactor. Environ Sci Technol 48(20):12181–12189. https://doi.org/10.1021/es501966h

13. Liu Z, Adewuyi YG, Shi S, Chen H, Li Y, Liu D, Liu Y (2019) Removal of gaseous Hg0 using novel seaweed biomass-based activated carbon. Chem Eng J 366:41–49. https://doi.org/10.1016/j.cej.2019.02.025
14. Outridge PM, Mason RP, Wang F, Guerrero S, Heimburger-Boavida LE (2018) Updated Global and Oceanic Mercury Budgets for the United Nations Global Mercury Assessment 2018. Environ Sci Technol 52(20):11466–11477. https://doi.org/10.1021/acs.est.8b01246
15. Presto AA, Granite EJ (2007) Impact of sulfur oxides on mercury capture by activated carbon. Environ Sci Technol 41(18):6579–6584. https://doi.org/10.1021/es0708316
16. Puziy AM, Poddubnaya OI, Socha RP, Gurgul J, Wisniewski M (2008) XPS and NMR studies of phosphoric acid activated carbons. Carbon 46(15):2113–2123. https://doi.org/10.1016/j.carbon.2008.09.010
17. Qiu K, Zhou J, Qi P, Zhou Q, Gao X, Luo Z (2017) Experimental study on ZnO-TiO2 sorbents for the removal of elemental mercury. Korean J Chem Eng 34(9):2383–2389. https://doi.org/10.1007/s11814-017-0154-6
18. Qu W, Liu J, Shen F, Wei P, Lei Y (2016) Mechanism of mercury-iodine species binding on carbonaceous surface: Insight from density functional theory study. Chem Eng J 306:704–708. https://doi.org/10.1016/j.cej.2016.07.115
19. Reddy BM, Durgasri N, Kumar TV, Bhargava SK (2012) Abatement of Gas-Phase Mercury—Recent Developments. Catal Reviews 54(3):344–398. https://doi.org/10.1080/01614940.2012.650966
20. Sano A, Takaoka M, Shiota K (2017) Vapor-phase elemental mercury adsorption by activated carbon co-impregnated with sulfur and chlorine. Chem Eng J 315:598–607. https://doi.org/10.1016/j.cej.2017.01.035
21. Sun P, Zhang B, Zeng X, Luo G, Li X, Yao H, Zheng C (2017) Deep study on effects of activated carbon's oxygen functional groups for elemental mercury adsorption using temperature programmed desorption method. Fuel 200:100–106. https://doi.org/10.1016/j.fuel.2017.03.031
22. Tao S, Li C, Fan X, Zeng G, Lu P, Zhang X, Wen Q, Zhao W, Luo D, Fan C (2012) Activated coke impregnated with cerium chloride used for elemental mercury removal from simulated flue gas. Chem Eng J 210:547–556. https://doi.org/10.1016/j.cej.2012.09.028
23. Tong L, Yue T, Zuo P, Zhang X, Wang C, Gao J, Wang K (2017) Effect of characteristics of KI-impregnated activated carbon and flue gas components on Hg-0 removal. Fuel 197:1–7. https://doi.org/10.1016/j.fuel.2016.12.083
24. Xu Y, Cao L, Sun W, Yang J (2017) In-situ catalytic oxidation of Hg0 via a gas diffusion electrode. Chem Eng J 310:170–178. https://doi.org/10.1016/j.cej.2016.10.095
25. Yan R, Liang DT, Tsen L, Wong YP, Lee YL (2004) Bench-scale experimental evaluation of carbon performance on mercury vapour adsorption. Fuel 83(17–18):2401–2409. https://doi.org/10.1016/j.fuel.2004.06.031
26. Yang H, Xu Z, Fan M, Bland AE, Judkins RR (2007) Adsorbents for capturing mercury in coal-fired boiler flue gas. J Hazard Mater 146(1–2):1–11. https://doi.org/10.1016/j.jhazmat.2007.04.113

27. Yang J, Li Q, Li M, Zhu W, Yang Z, Qu W, Hu Y, Li H (2020) In Situ Decoration of Selenide on Copper Foam for the Efficient Immobilization of Gaseous Elemental Mercury. Environ Sci Technol 54(3):2022–2030. https://doi.org/10.1021/acs.est.9b07057
28. Yang J, Zhu W, Qu W, Yang Z, Wang J, Zhang M, Li H (2019) Selenium Functionalized Metal-Organic Framework MIL-101 for Efficient and Permanent Sequestration of Mercury. Environ Sci Technol 53(4):2260–2268. https://doi.org/10.1021/acs.est.8b06321
29. Yang S, Wang D, Liu H, Liu C, Xie X, Xu Z, Liu Z (2019) Highly stable activated carbon composite material to selectively capture gas-phase elemental mercury from smelting flue gas: Copper polysulfide modification. Chem Eng J 358:1235–1242. https://doi.org/10.1016/j.cej.2018.10.134
30. Yang Z, Li H, Liu X, Li P, Yang J, Lee P-H, Shih K (2018) Promotional effect of CuO loading on the catalytic activity and SO2 resistance of MnOx/TiO2 catalyst for simultaneous NO reduction and Hg0 oxidation. Fuel 227:79–88. https://doi.org/10.1016/j.fuel.2018.04.074
31. Yang Z, Li H, Yang Q, Qu W, Zhao J, Feng Y, Hu Y, Yang J, Shih K (2020) Development of selenized magnetite (Fe 3 O 4?x Se y) as an efficient and recyclable trap for elemental mercury sequestration from coal combustion flue gas. *Chemical Engineering Journal*, *394*, Article 125022. https://doi.org/10.1016/j.cej.2020.125022
32. Yao Y, Velpari V, Economy J (2014) Design of sulfur treated activated carbon fibers for gas phase elemental mercury removal. Fuel 116:560–565. https://doi.org/10.1016/j.fuel.2013.08.063
33. Zhang J, Duan Y, Zhou Q, Zhu C, She M, Ding W (2016) Adsorptive removal of gas-phase mercury by oxygen non-thermal plasma modified activated carbon. Chem Eng J 294:281–289. https://doi.org/10.1016/j.cej.2016.02.002
34. Zhao J, Li H, Yang Z, Zhu L, Zhang M, Feng Y, Qu W, Yang J, Shih K (2018) Dual Roles of Nano-Sulfide in Efficient Removal of Elemental Mercury from Coal Combustion Flue Gas within a Wide Temperature Range. Environ Sci Technol 52(21):12926–12933. https://doi.org/10.1021/acs.est.8b04340
35. Zheng J-M, Shah KJ, Zhou J-S, Pan S-Y, Chiang P-C (2017) Impact of HCl and O-2 on removal of elemental mercury by heat-treated activated carbon: Integrated X-ray analysis. *Fuel Processing Technology*, *167*, 11-17. https://doi.org/10.1016/j.fuproc.2017.06.017
36. Zhong L, Li W, Zhang Y, Norris P, Cao Y, Pan W-P (2017) Kinetic studies of mercury adsorption in activated carbon modified by iodine steam vapor deposition method. Fuel 188:343–351. https://doi.org/10.1016/j.fuel.2016.10.048
37. Zhou J, Cao L, Wang Q, Tariq M, Xue Y, Zhou Z, Sun W, Yang J (2019) Enhanced Hg0 removal via α-MnO2 anchored to MIL-96(Al). Appl Surf Sci 483:252–259. https://doi.org/10.1016/j.apsusc.2019.03.261
38. Zhu Y, Han X, Huang Z, Hou Y, Guo Y, Wu M (2018) Superior activity of CeO2 modified V2O5/AC catalyst for mercury removal at low temperature. Chem Eng J 337:741–749. https://doi.org/10.1016/j.cej.2017.10.115

Figures

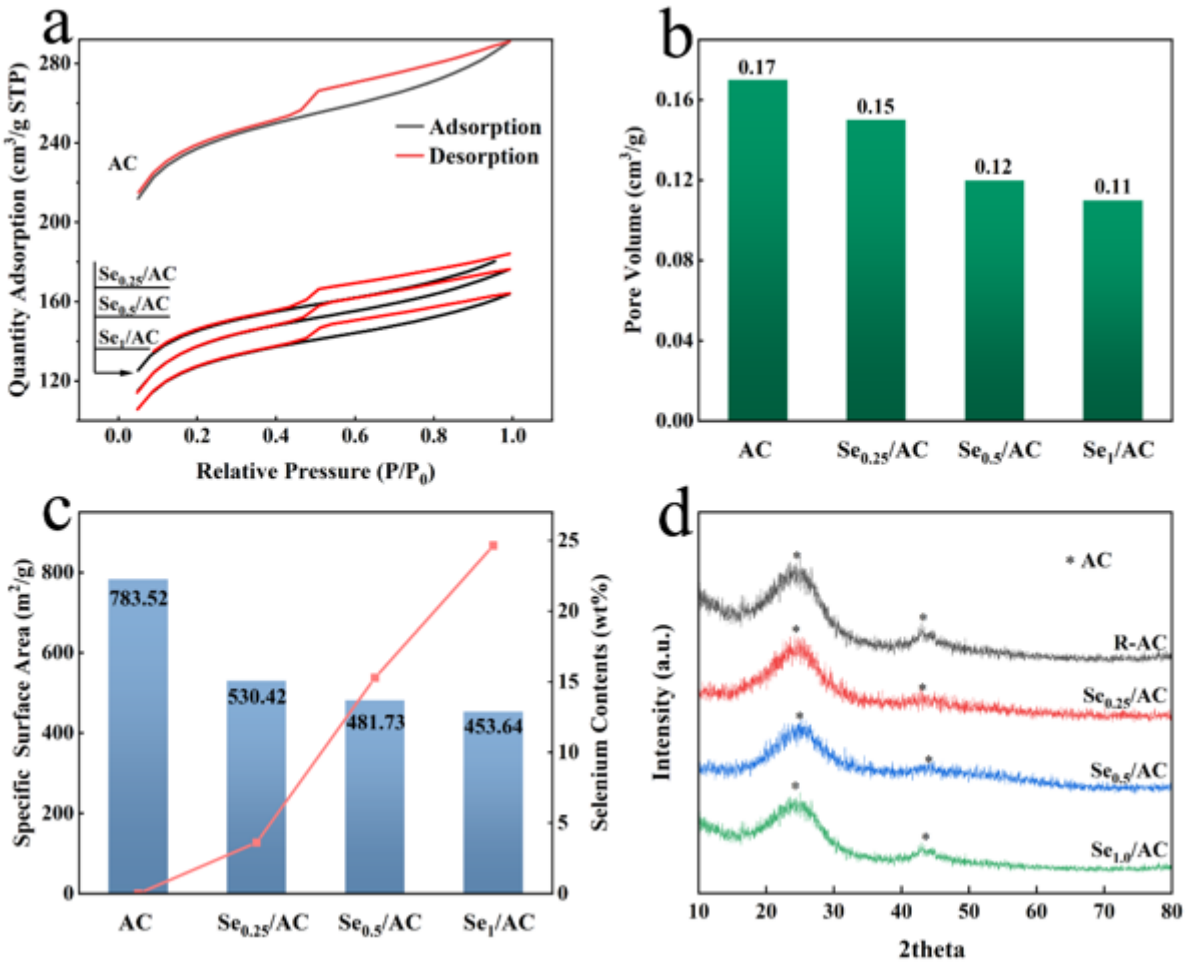

Figure 1

(a) adsorption-desorption curve, (b) pore volume, (c) specific surface area and selenium contents, and (d) XRD of all sorbents

Figure 2

The SEM of samples: (a) R-AC, (b)$Se_{0.25}$/AC

Figure 3

Diagrammatical illustration of Hg^0 removal system.

Figure 4

(a) 12h Hg^0 removal efficiency of different samples, (b) Hg^0 adsorption penetration experiments of Sex/AC, (c) 72h Hg^0 removal efficiency of different temperature, (d) Hg^0 adsorption penetration experiments of different temperature, (e) Hg^0 removal efficiency of various O_2 concentrations, (e) Hg^0 removal efficiency of N_2+NO and N_2+SO_2.

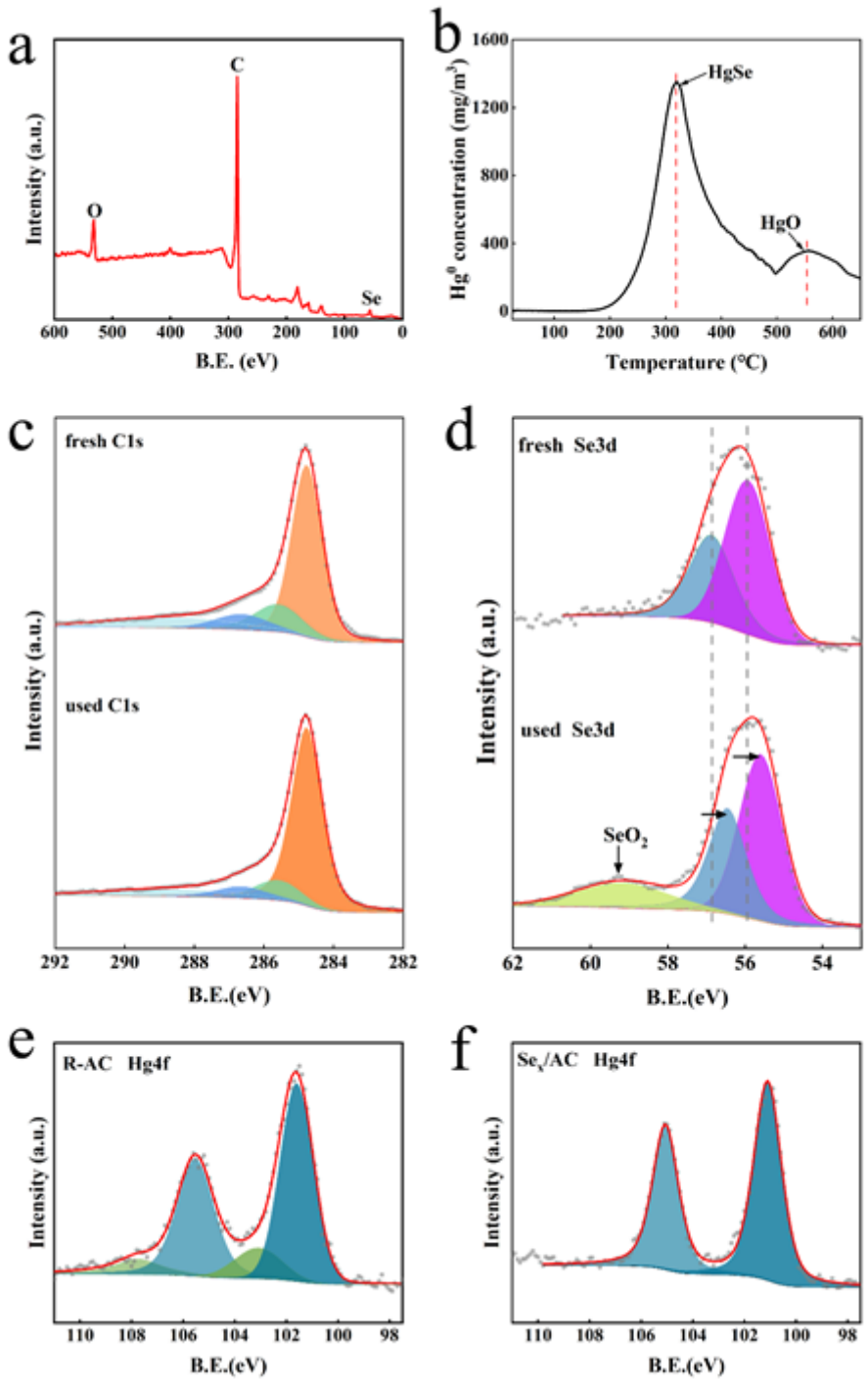

Figure 5

(a) the XPS full spectrum, (b) the Hg-TPD pattern of used $Se_{0.5}$/AC, (c) C1s XPS spectra of fresh and used Se_x/AC, (d) Se3d XPS spectra of fresh and used Se_x/AC, (e)(f) Hg4f XPS spectra of R-AC and Se_x/AC

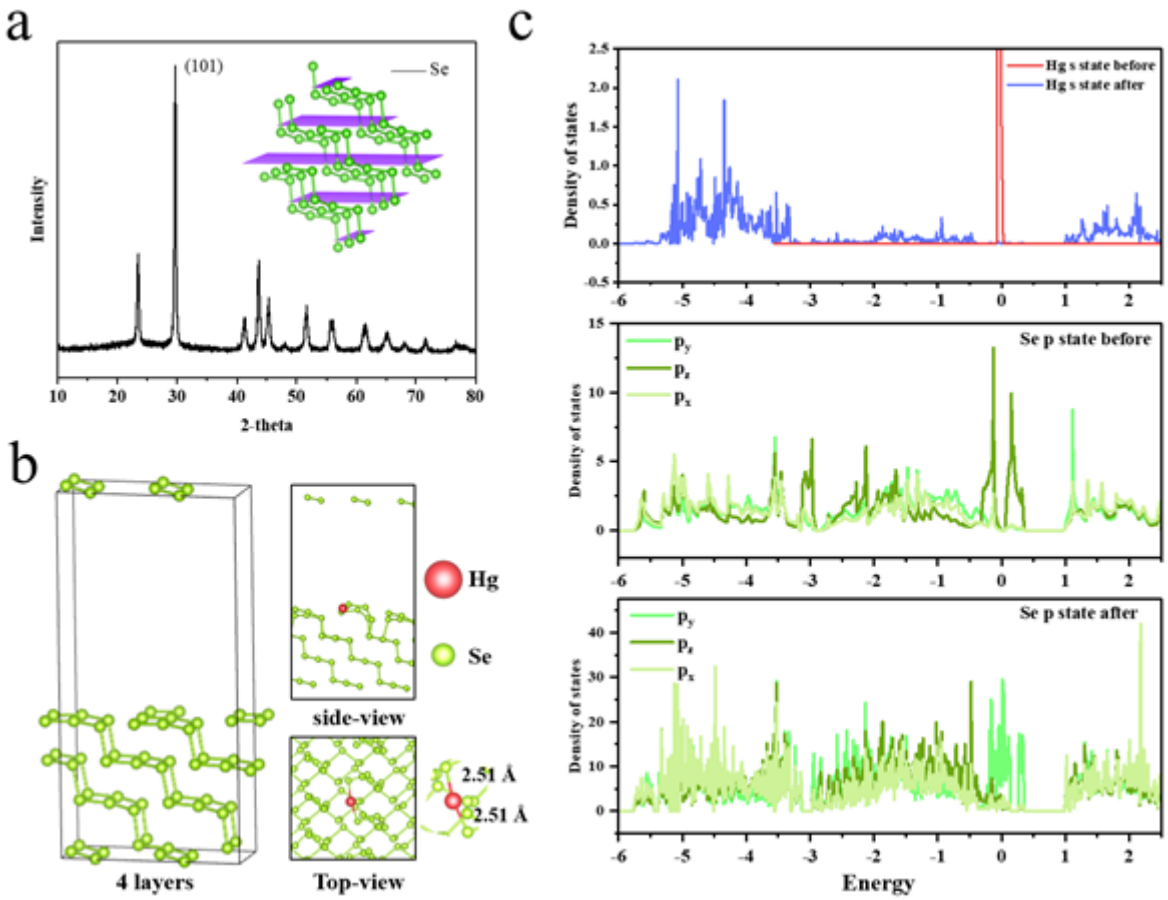

Figure 6

(a) the XRD pattern of Se powder, illustration represent the 101 face of the Se crystal. (b) Optimized adsorption model of Se slab and mercury adsorption model. (c) The partial density of states of Hg s state and the Se p state.

Supplementary Files

This is a list of supplementary files associated with this preprint. Click to download.

- GraphicalAbstract.png
- Supportinginformation.docx